Title

Ab initio dynamics and photoionization mass spectrometry reveal ion–molecule pathways from ionized acetylene clusters to benzene cation

Journal

Proceedings of the National Academy of Sciences of the United States of America, 114(21)

ISSN

0027-8424

Authors

Stein, Tamar
Bandyopadhyay, Biswajit
Troy, Tyler P
et al.

Publication Date

2017-05-23

DOI

10.1073/pnas.1616464114

Peer reviewed

Classification: physical science, chemistry.

Ab initio dynamics and photoionization mass spectrometry reveal ion-molecule pathways from ionized acetylene clusters to benzene cation

Tamar Stein [1,2*], Biswajit Bandyopadhyay[1*],

Tyler Troy[1], Yigang Fang[1], Oleg Kostko[1],

Musahid Ahmed[1†], and Martin Head-Gordon[1,2†]

[1] Chemical Sciences Division, Lawrence Berkeley National Laboratory, 1 Cyclotron Road, Berkeley, California - 94720, United States

[2] Department of Chemistry, University of California Berkeley, Berkeley, California-94720, United States

* Equal contributions

[†]M.H.-G.: E-mail: mhg@cchem.berkeley.edu, [†]M. A.: E-mail: MAhmed@lbl.gov.

Keywords: Ion-molecule reactions, polycyclic aromatic hydrocarbons, molecular dynamics.

Abstract

The growth mechanism of hydrocarbons in ionizing environments such as the interstellar medium (ISM), and some combustion conditions remains incompletely understood. Ab-initio molecular dynamics (AIMD) simulations and molecular beam vacuum-ultraviolet (VUV) photoionization mass spectrometry experiments were performed to understand the ion-molecule growth mechanism of small acetylene clusters (up to hexamers). A dramatic dependence of product distribution on the ionization conditions is demonstrated experimentally and understood from simulations. The products change from reactive fragmentation products in a higher temperature, higher density gas regime towards a very cold collision-free cluster regime that is dominated by products whose empirical formula is $(C_2H_2)_n^+$, just like ionized acetylene clusters. The fragmentation products result from reactive ion-molecule collisions in a comparatively higher pressure and temperature regime followed by unimolecular decomposition. The isolated ionized clusters display rich dynamics that contain bonded $C_4H_4^+$ and $C_6H_6^+$ structures solvated with one or more neutral acetylene molecules. Such species contain large amounts (> 2 eV) of excess internal energy. The role of the solvent acetylene molecules is to affect the barrier crossing dynamics in the potential energy surface (PES) between $(C_2H_2)_n^+$ isomers and provide evaporative cooling to dissipate the excess internal energy and stabilize products including the aromatic ring of the benzene cation. Formation of the benzene cation is demonstrated in AIMD simulations of clusters of acetylene clusters with n>3, as well as other metastable $C_6H_6^+$ isomers. These results suggest a new path for aromatic ring formation in cold acetylene-rich environments such as parts of the ISM.

Significance statement

The formation of benzene and its cation constitute a likely gateway to polycyclic aromatic hydrocarbons, which are the bridge to larger carbonaceous material such as soot in combustion processes and interstellar dust. Our paper reports new computational and experimental results that address the long-standing puzzle of how ion-molecule reactions involving small unsaturated organics, such as acetylene, which is widespread in the interstellar medium, can lead to benzene cation. We present new insights into the facile way in which $C_6H_6^+$ products, including benzene cation, can be accessed after ionization of cold isolated neutral clusters, and show that there is a catalytic role for what are nominally spectator acetylene molecules!

Introduction

The growth mechanism of longer chain and polycyclic aromatic hydrocarbons is of importance in astrochemistry, where polycyclic aromatic hydrocarbons (PAHs) (fused benzene rings) are known to be widely distributed across the interstellar medium (ISM).(1, 2) PAHs, in fact, are thought to be the most abundant molecule in the ISM after H_2 and CO.(3) PAHs are also by-products of fuel combustion processes, and the mechanism for their formation is also of interest in the combustion community, not least because of the environmental and health impacts associated with their carcinogenic and mutagenic nature.(4, 5) Much research has focused on minimizing their formation by varying combustion conditions, aiming for cleaner combustion processes. More generally, PAHs can be viewed as a bridge or intermediate stage between small organic precursor molecules, such as acetylene, and larger carbonaceous materials such as interstellar dust in the ISM(6) or soot in combustion processes.(7) In turn, benzene is the gateway to PAHs from smaller hydrocarbons.

Several mechanisms have been proposed to explain PAHs growth,(8-13) typically based on coupling reactions between stable species like acetylene and reactive aromatic radicals. A prominent example is the well-known hydrogen abstraction C_2H_2 addition (HACA) mechanism, which is composed of two sequential steps. First, hydrogen abstraction from an aromatic occurs (via another radical), activating the aromatic molecule into an aryl radical. This step is followed by the addition of an acetylene unit to the aryl radical, giving it a C_2 sidechain. Repetition of these two basic steps can lead to larger PAHs. Recently, ion polymerization from clusters has also been suggested as a pathway for PAH generation.(14, 15) Several studies have focused on the formation of naphthalene, suggesting it forms via reaction of the phenyl radical with vinylacetylene.(16) In addition, the formation of the naphthalene cation from ion-molecule reactions such as the benzene cation and the ethynyl radical has been examined.(17)

Benzene is the basic building block of PAHs, and different pathways for the formation of benzene have been proposed which depend on the chemical and physical environment.(18, 19) The first synthesis of benzene goes back to Berthelot's experiment in 1867, where aromatic materials were isolated upon heating acetylene.(13) It was

speculated that the multi-step process was initiated by isomerization of acetylene to vinylcarbene, which reacts with acetylene to form vinylacetylene.(20) Repetition of the carbene formation step and the acetylene insertion step can further lead to hexa-1,3-dien-5-yne that can cyclize to form benzene.(21) In soot formation, extensive work has been done on the formation of the first aromatic molecule.(7) Among the proposed reactions, recombination of propargyl radicals is believed to be an important step that leads(22) to cyclic products such as benzene and C_6H_5.(23, 24) Other important radical reactions include reactions of C_4H_3 and C_4H_5 with acetylene.(25-27) In cooler environments, astrochemical models suggest formation of benzene mainly from ion-molecule reactions.(28-31) It has also been suggested that the formation of benzene can proceed via barrier-less radical reaction of ethynyl radical and 1,3-butadiene.(30, 32) Other studies focused on the formation of benzene and other organic molecules upon irradiation of acetylene ices.(22, 33) Notwithstanding this progress, the formation of benzene (or its cation) in the ISM is still not fully understood.

Mass spectrometry is a versatile tool to study the chemistry of clusters and characterize the reaction products produced in molecular beams, and hence has been applied to photoionization or electron impact ionization of acetylene clusters. Depending on the initial conditions, the resulting ions detected in the experiments were either fragmentation products or ionized intact clusters of the form $(C_2H_2)_n^+$.(34-37) Among studies that showed intact clusters, substantial signal was detected at m/z 78 and attributed to $(C_2H_2)_3^+$.(38) The structure of the $(C_2H_2)_3^+$ ion proved controversial, suggestions being benzene(39) or benzvalene.(36) It was suggested that exothermic processes leading to benzene cation formation will result in evaporation of neutral acetylene molecules.(34, 36, 38, 39) Additional indications that the $(C_2H_2)_3^+$ structure is benzene cation came from mass spectrometry combined with ion mobility measurements(40) and from comparison to deprotonation rate measurements of the benzene cation in water.(41) However, vibrational predissociation spectra concluded that other isomers could contribute to $C_6H_6^+$, with the dominant one being C_2H_2 coordinated to a $C_4H_4^+$ core.(42) These results suggest that reaction conditions are of critical importance.

In this work we present a comprehensive study combining experiment and theory to elucidate the mechanism of carbon growth arising from ionization of neutral acetylene clusters. We performed an ab-initio study on the structures of small acetylene clusters (up to hexamers) both on the neutral and cationic potential energy surface (PES) together with molecular dynamics simulations of the ionized clusters. We present VUV molecular beam photoionization experiments in which the ionization occurs at various distances from the nozzle exit.(43) The experimental setup enables us to distinguish between products resulting from ionization of clusters and products resulting from post ionization ion-molecule reactions.(44) We will show that ionization of neutral acetylene clusters results in effectively barrierless formation of covalently bonded $C_4H_4^+$ and $C_6H_6^+$ species, complexed to the remaining acetylene molecules. The additional acetylene molecules are shown to stabilize the bonded products, and also provide an additional pathway for dissipation of the reaction energy associated with $C_4H_4^+$ and $C_6H_6^+$ formation by their evaporation. Furthermore, using ab initio molecular dynamics simulations, we will show that the benzene cation is formed and is evaporatively stabilized upon ionization of clusters larger than the trimer.

Results and discussion

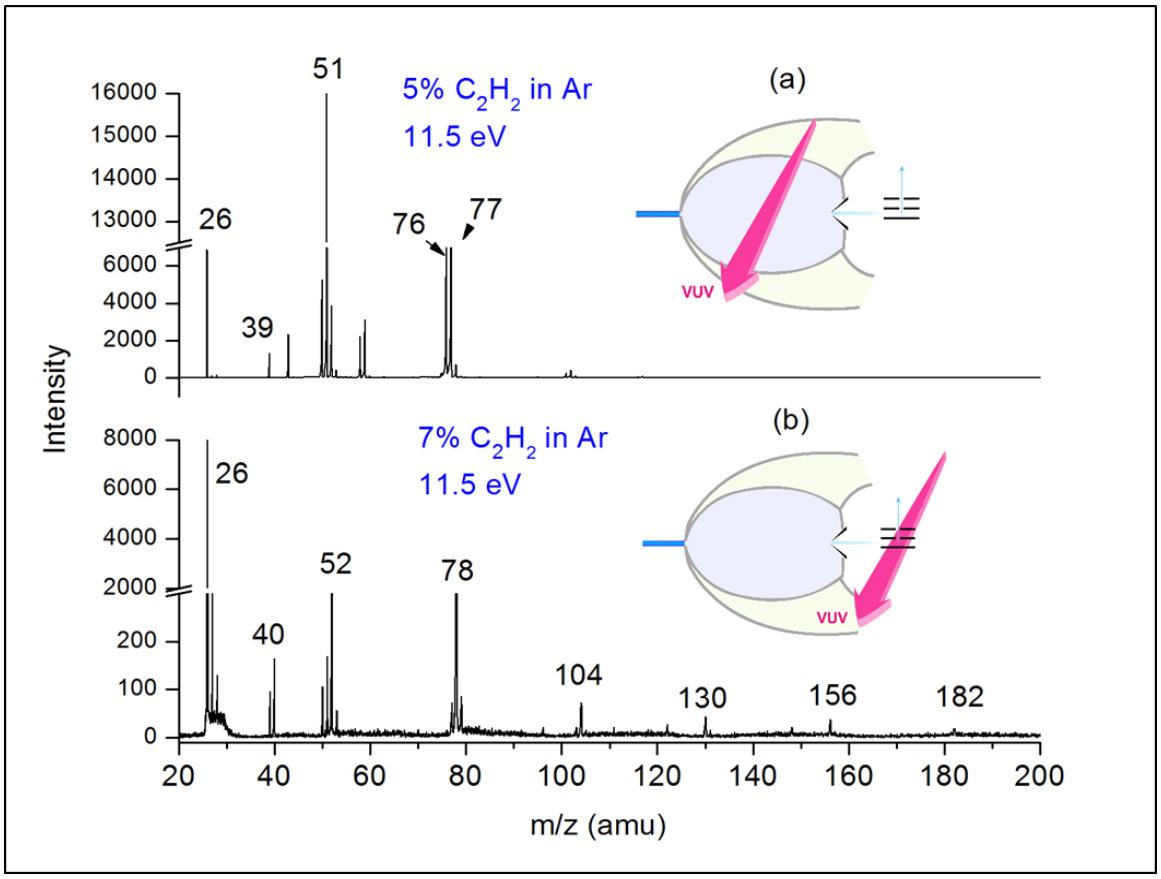

Figure 1: Mass spectra of acetylene clusters obtained from in-source (a) and mass-spec ionization (b) at 11.5 eV. The experimental schemes are graphically shown in the insets. While in-source ionization shows fragmented acetylene clusters (e.g. $C_4H_3^+$, $C_6H_5^+$), mass-spec ionization shows intact clusters in the form of $(C_2H_2)_n^+$.

Figure 1(a) and (b) depict representative mass spectra of acetylene clusters obtained from in-source and mass-spec ionizations, respectively. At 2 mm in-source ionization, we see primarily fragmentation products whose stoichiometry is $(C_2H_2)_nC_2H^+$ and $(C_2H_2)_{n-2}C_2^+$ (Fig. 1a). For the mass-spec ionization with 7% acetylene-argon mixture we observe products with stoichiometry corresponding to intact $(C_2H_2)_n^+$ clusters (Fig. 1b). We have used different backing pressures and observed that higher pressure produced larger clusters along with an overall increase of intensities of all the ions (full results to be published separately). The mass-spec ionization spectrum is consistent with Kocisek et. al's electron impact ionization experiments which yielded intact acetylene clusters unless the acetylene concentration was very low (0.7%).(37)

Figure 1 shows a pronounced difference in the experimental mass spectrum obtained when ionization occurs at closer versus farther distances from the nozzle exit. While the dominant products close to the nozzle exit (in-source ionization) are fragmentation products, at large distances (mass spec. ionization) the dominant products are ionized intact clusters. In the supersonic expansion, the number density as well as the temperature decrease drastically within few nozzle diameters along the propagation direction of the beam, and it is well established that the collision rate is maximal at the nozzle throat.(45) Thus ion-molecule reactions are expected to be dominant when ionization occurs close to the nozzle exit. From the results, it is evident that in this regime, product fragmentation typically occurs before detection. In previous work, we studied the structures that result from fragmentation of the dimer.(44) On the neutral surface, the dimer is either a T-shaped structure or a slipped parallel structure, which move on the cation surface after ionization to yield bonded structures with high internal energy.(44) The excess energy leads to unimolecular decomposition, such as H loss or methyl loss; we previously characterized some of those fragmentation pathways.(44)

On the other hand, at large distances from the nozzle exit, cold neutral clusters are ionized in a collision-free environment.(44) From Figure 1, evidently, there is a much larger probability of detecting intact $C_4H_4^+$ and $C_6H_6^+$ products in this regime. These results are in agreement with experiments done by El-Shall and coworkers who also observed large peaks for intact clusters, among them the $C_6H_6^+$ peak at 78 m/z, which was attributed to the benzene cation.(40) They have also performed a series of experiments to probe the structure of the $C_4H_4^+$ and $C_6H_6^+$ products such as ion mobility measurements(40, 46) and stepwise hydration experiments.(41, 46) Their studies support assignment of the $C_6H_6^+$ structure to the benzene cation. For the $C_4H_4^+$ isomer they found evidence for several structures, with cyclobutadiene being predominant. Moreover, they assigned their $C_8H_8^+$ peak based on ion mobility experiments as being due to the benzene$^+$ acetylene complex, and suggest it is a result of ionization of the tetramer cluster.(47) Booze et al (36) also observed intact cluster formation, and suggested that the $C_6H_6^+$ produced from the trimer is of the form $C_4H_4^+$-C_2H_2 which later stabilizes by evaporation of the monomer, without forming a covalently bonded $C_6H_6^+$ structure. In the same manner, they suggested that the $C_8H_8^+$ produced from the tetramer is of the form

$C_6H_6^+$-C_2H_2 which stabilizes by evaporation of acetylene, without forming a covalently bonded $C_8H_8^+$ structure. Differences in ionization energies measured in photoionization efficiency curves also allow us to separate the mechanistic details for both processes, as shown in the supplementary information (Figure S1). For in-source ionization, we see very little evidence of dimers and trimers formed below the ionization energy of acetylene monomer, while for mass spec ionization there is formation of dimers and trimers well below this limit.

To understand the striking difference between the two sets of experimental results at an atomistic level, we turn to the computational results, beginning with stable neutral acetylene clusters that are then ionized. Figure 2 shows the low-energy structures of the neutral trimer (Tr), tetramer (T) and pentamer (P) clusters of acetylene and their binding energies with respect to free acetylene molecules (three, four and five respectively). (Figure S2 illustrates the isomers of the hexamer). The optimized structures are dominated by T-shaped CH-π pair-wise interactions in which a partially positively charged hydrogen points toward the π electron cloud of the second acetylene. For the trimer, in structure Tr(a) the CH-π interactions are maximized (there are three versus only two in structure Tr(b)), and consequently structure Tr(a) is lower in energy by 7.5 kJ/mol than structure Tr(b). It is also evident that the CH-π interaction governs the structure of the larger neutral clusters.

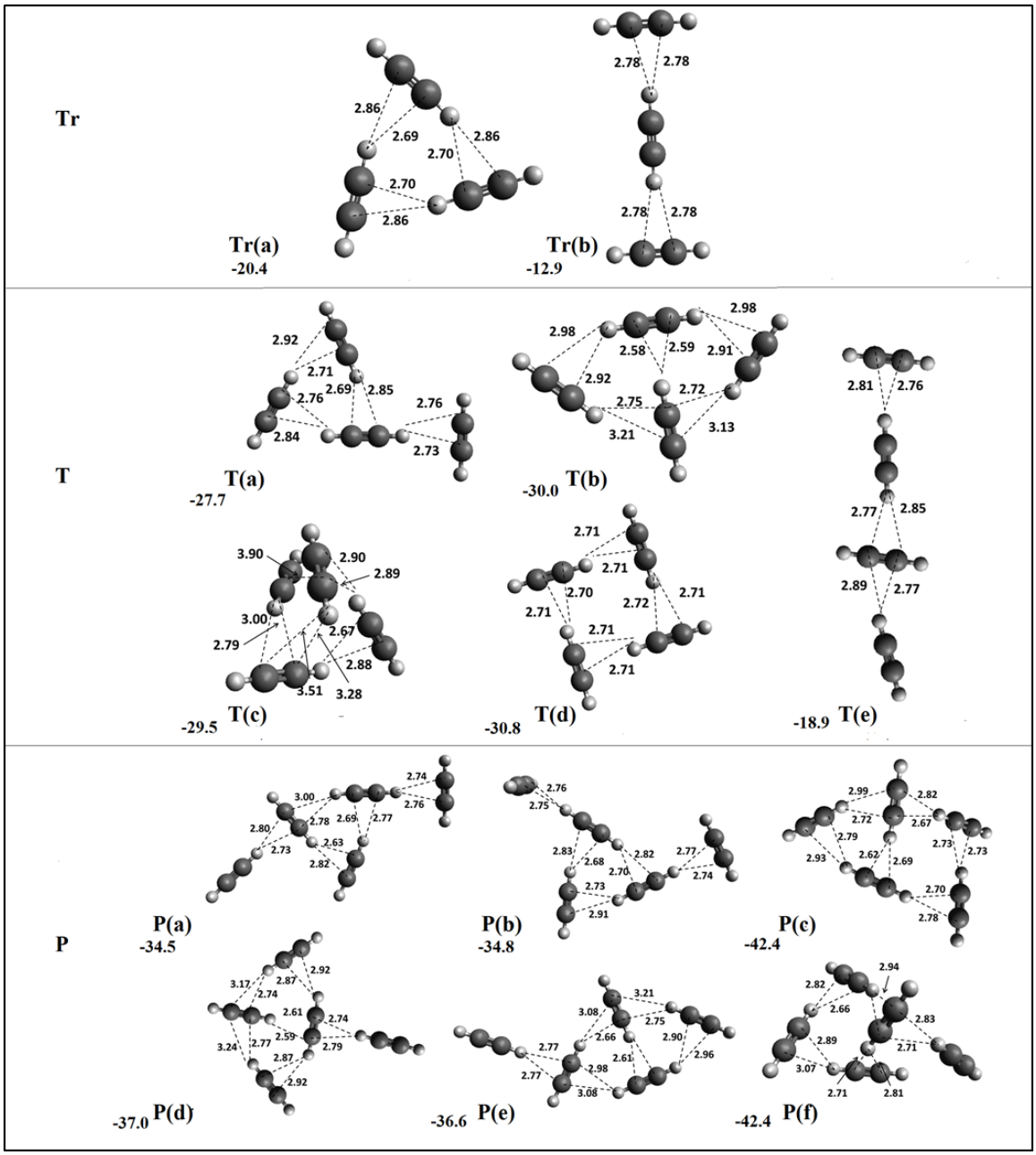

Figure 2: Optimized low-energy structures of neutral acetylene clusters. Tr: trimer structures, T: tetramer structures, P: pentamer structures. Binding energies (kJ/mol) are shown for each relaxed structure.

Upon ionization, the neutral cluster geometry is non-optimal, and the atoms relax on the cationic PES. The top panel of Figure 3 shows the structure obtained when relaxing the neutral trimer structure, Tr(a) (see Figure 2), on the cationic surface. This Tr structure resembles the bonded first encounter complex (FEC) reported on the $C_4H_4^+$

surface,(44, 48) complexed with the third acetylene unit, which is stabilized through CH-π interactions as discussed above. The structures resulting from relaxing the tetramer and pentamer clusters on the cation PES are also shown in Figure 3 (T and P), and are covalently bonded structures complexed to the remaining acetylene molecules.

Interestingly, for the case of the tetramer and pentamer clusters, we not only see formation of $C_4H_4^+$ structures, but we also found downhill pathways for formation of bonded $C_6H_6^+$ structures. These $C_6H_6^+$ structures form without a barrier, upon ionization of the neutral structures. Direct pathways to $C_6H_6^+$ formation, without the need for a $C_4H_4^+$ intermediate, upon ionization of the neutral n>3 Van der Waals clusters is a very surprising result. The differing neutral geometries of the larger cluster in several cases enables access to $C_6H_6^+$ structures that cannot be barrierlessly accessed from the trimer. The resulting $C_6H_6^+$ isomers look like a FEC for three acetylene units; an allyl-cyclopropenyl cation shown in Figure 3 (T(a) and T(d)), and a vinyl-cyclobutadienyl cation shown in Figure 3 (P(d)).

Additionally, while the $C_4H_4^+$ structure that is directly formed after ionization of the trimer was an FEC-like structure, the $C_4H_4^+$ structure that is accessed by a downhill pathway upon ionization of the tetramer and pentamer clusters (as well as for hexamers) is the cyclobutadiene isomer – virtually the global minimum on the $C_4H_4^+$ PES. A barrierless pathway to cyclobutadiene means that the presence of the additional acetylene units has modified the potential energy surface to remove the barrier that exists between the FEC and cyclobutadiene on the dimer and trimer surfaces. The solvation effect of the additional acetylene units thus is also a catalytic effect.

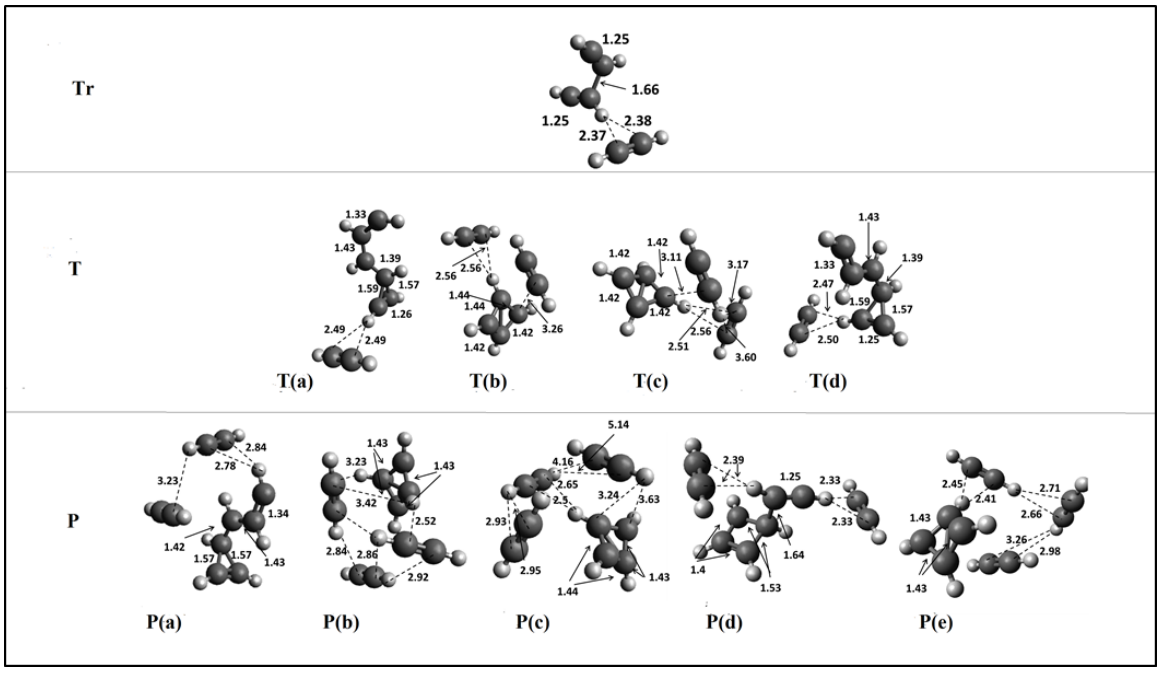

Figure 3: Structures of the ionized clusters upon relaxation starting from each optimized neutral structure shown in Figure 2. The isomer labels correspond to those shown in Figure 2. Tr: resulting trimer structures, T: resulting tetramer structures, P: resulting pentamer clusters.

The structures of the solvated ionized complexes suggests a mechanism for dissipating their excess internal energy. While containing a large amount of energy after ionization, the covalently bonded core can be stabilized by evaporating the remaining complexed acetylene molecules. The departing acetylene molecules must do work to overcome their binding energy, and additionally may carry away excess kinetic energy. These are the reasons to expect the formation of stable $C_4H_4^+$ and $C_6H_6^+$ species as is observed in the experimental mass spectra results shown in Figure 1b.

To obtain deeper insight into the processes that occur after the ionization of the clusters, we performed AIMD simulations. The simulations start from the different neutral cluster structures (shown in Figure 2), and proceed on the cation PES, thereby providing the system with a large amount of internal energy. An estimate of this energy can be obtained from comparison of the vertical ionization energy (IE) to the adiabatic IE as shown in the Supplementary Material Table S1. While the trimer contains almost 2 eV of excess internal energy, the tetramer and pentamer clusters contain above 4 eV of excess internal energy, which approaches the binding energy of a single chemical bond.

Even more internal energy is generated as chemical dynamics on the cation surface accesses more stable isomers.

For all cluster sizes, the majority of the short 1.2 ps trajectories resulted in a covalently linked $C_4H_4^+$ structure, which may be complexed to some or all of the remaining acetylene molecules. For the trimer clusters, among 60 trajectories, 80% ended in this channel, either as cyclobutadiene (39 trajectories) or as methylenecyclopropene (9 trajectories). Similarly, from the 150 tetramer trajectories, 79% (118 trajectories) resulted in a covalently linked $C_4H_4^+$ core, either as cyclobutadiene (87 trajectories) or methylenecyclopropene (31 trajectories). The same trend is seen for the pentamer and hexamer clusters where about 70% of the trajectories ended with bonded $C_4H_4^+$ structures, mostly as cyclobutadiene or methylenecyclopropane. For the trimer, the nascent $C_4H_4^+$ structures are complexed to one additional acetylene molecule that can evaporate and carry with it the extra energy – leading to stable $C_4H_4^+$ structures or to a stable $C_4H_4^+$ structure complexed to an acetylene molecule – in agreement with vibrational predissociation spectra study by Relph et. al. (42).

The rest of the trajectories formed a covalently linked $C_6H_6^+$ structure. In the trimer case, 20% (15 out of 60) of the trajectories ended on the $C_6H_6^+$ PES with 1 trajectory leading to the formation of benzene cation on the 1.2 ps timescale. The path to the benzene cation from the trimer is shown in Figure 4, which shows some significant structures that appear along the trajectory (bottom panel) and the corresponding stationary points on the PES (top panel). One can see the formation of the allyl-cyclopropenyl structure and its rearrangement, which leads to a benzvalene structure and then to the benzene cation. As shown in the PES, the transition from benzvalene cation to benzene cation goes through a 5 membered ring isomer in which the 6th carbon is above the plane of the ring and the barrier for the transition is 0.6 eV. The system has enough internal energy that the path to benzene formation involves only submerged barriers. 8 other trajectories reached the allyl-cyclopropenyl structure and could result in benzene cation if propagated for longer times. Nearly 9 eV of internal energy is associated with the benzene cation when it is formed from the trimer cation; more than enough to ensure fits fragmentation, unless it is stabilized by collisional or radiative energy transfer.

Despite the fact that the benzene cation is clearly accessed in the trimer trajectories, it is unlikely to survive because as already discussed above, the system is likely to fragment in order to dissipate its internal energy (unless it can live long enough to radiatively relax). In order for $C_6H_6^+$ to survive, it is not enough to have the energy to cross the entrance barrier: there needs to be an efficient way to dissipate the excess internal energy. At the chosen end-point of the tetramer trajectories (2.4 ps), 32 trajectories result in stable isomers with a bonded $C_6H_6^+$ core – about 21% of the total. As for the trimer, the formation of $C_6H_6^+$ can occur effectively barrierlessly by relaxation from the initial neutral cluster structures. As already discussed, the extra acetylene molecule perturbs not only the initial conditions but also the topology of the PES.

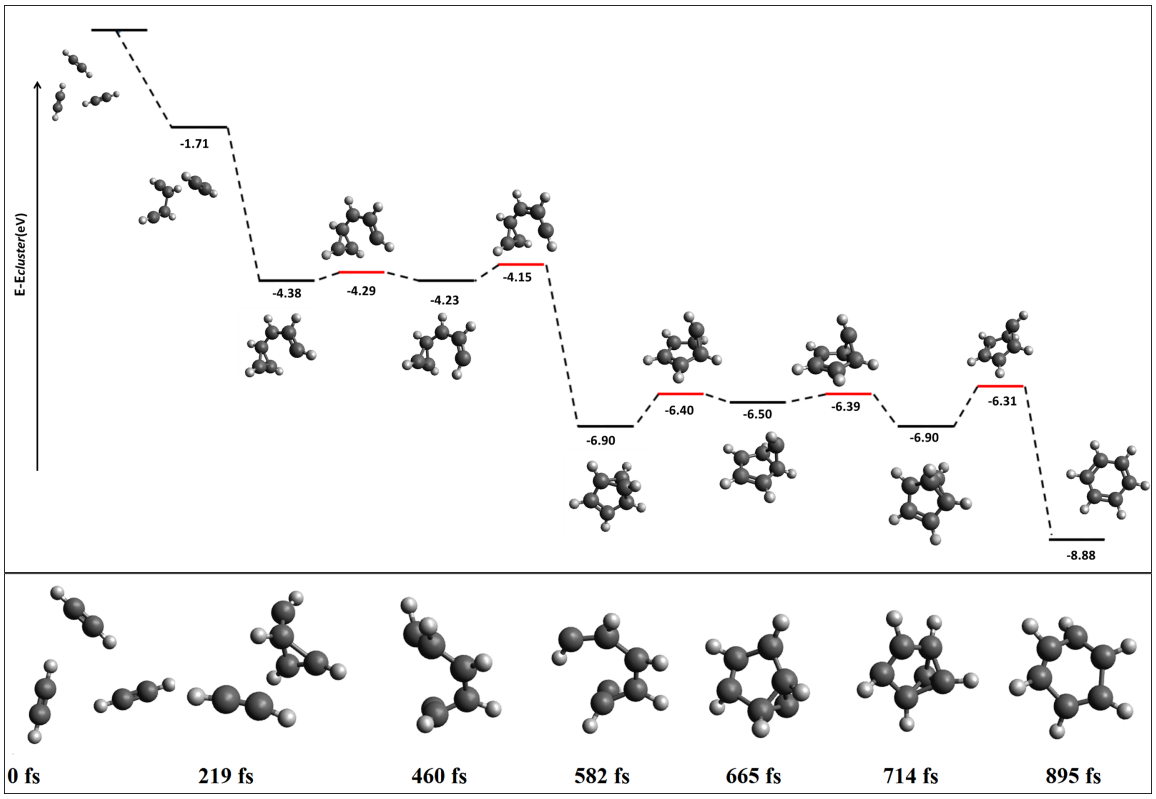

Figure 4: Top panel: Stationary points (saddle points in red) on a pathway leading to benzene cation from the ionized trimer cluster. Relative energies (eV) of the different structures are with respect to the initial cluster geometry. Bottom panel: Snapshots from a trajectory leading to benzene cation formation from the trimer cluster.

The most interesting question that the tetramer dynamics can address is the fate of the acetylene molecules that are solvating the hot nascent $C_4H_4^+$ or $C_6H_6^+$ core structures. For each trajectory, Figure 5 shows the time-dependence of the (shortest) C-C distance

between the acetylene that is most isolated from the $C_4H_4^+$ or $C_6H_6^+$ core (at the end of the simulation). It is clear that this distance grows with time. At around 0.7 ps, the separation to the most remote acetylene in all the trajectories is less than 10Å with the majority around 5Å. By contrast, at the end of the simulation, this distance is above 10Å for a majority of the trajectories, confirming that one acetylene molecule has detached from the cluster in these cases. Figure S4 shows the distance between the forming structure and the second-most remote acetylene unit (again defined at the end of the trajectory). In some, but not most trajectories, detachment of the second acetylene is observed. For the remainder of the trajectories, longer simulation times would be needed to determine if detachment occurs. The kinetic energy of the acetylene units is used to detach from the formed structure; the average kinetic energy at the end of the simulations is 0.23 eV. The average kinetic energy of the $C_6H_6^+$ and the $C_4H_4^+$ structure at the end of the simulations is 2.82 eV and 1.78 eV respectively.

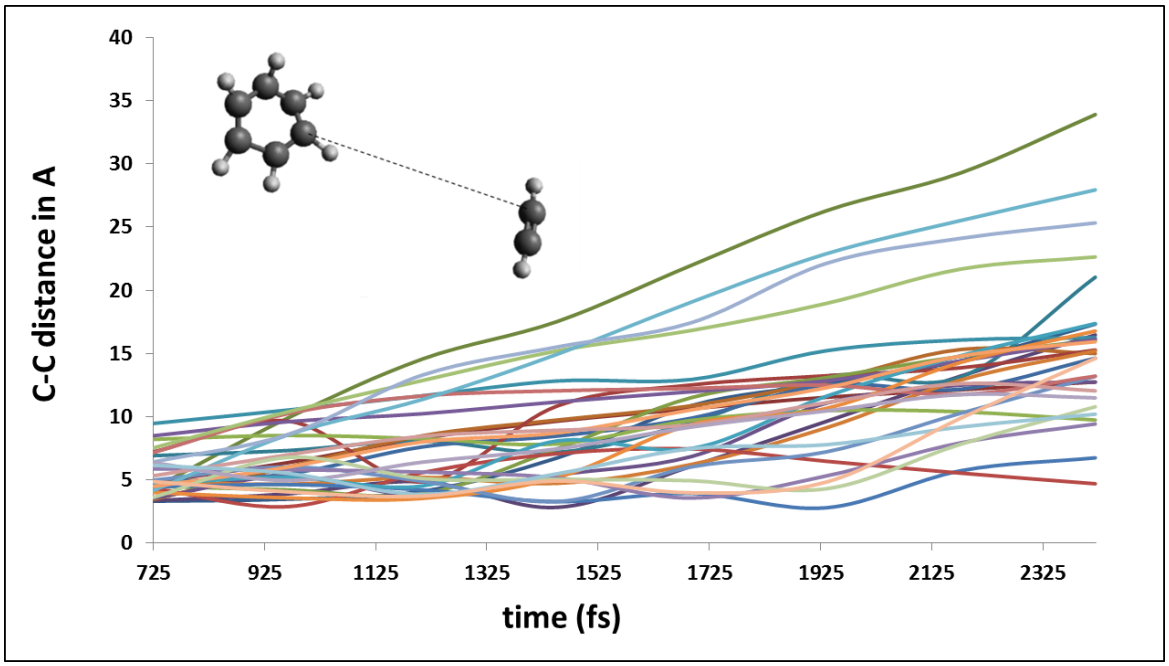

Figure 5: Time-dependence of the shortest CC distance between the nascent $C_4H_4^+$ or $C_6H_6^+$ structure and the most remote remaining acetylene molecule (which is defined at the end of the trajectory). An example of the CC distance is shown at the top left.

We find 6 tetramer trajectories that lead to the direct formation of benzene cation (all accessing this structure after more than 1.2 ps); one of them is presented in Figure 6.

In the example presented, the path to benzene cation goes through the Dewar benzene isomer. All six go through the allyl-cyclopropenyl and vinyl-cyclobutadienyl structures in the rearrangement process. Some cases also pass through other minima such as the Dewar benzene cation as illustrated in Figure 6 or the benzvalene cation. This result is very interesting since it reveals additional paths to benzene cation formation in rich acetylene environments. We also note that the structures at the end of 10 tetramer trajectories of the 32 that access $C_6H_6^+$ core resemble allyl-cyclopropenyl or vinyl-cyclobutadienyl cation. As noted above, these structures can access the benzene cation, so we expect some of them would ultimately lead to this isomer.

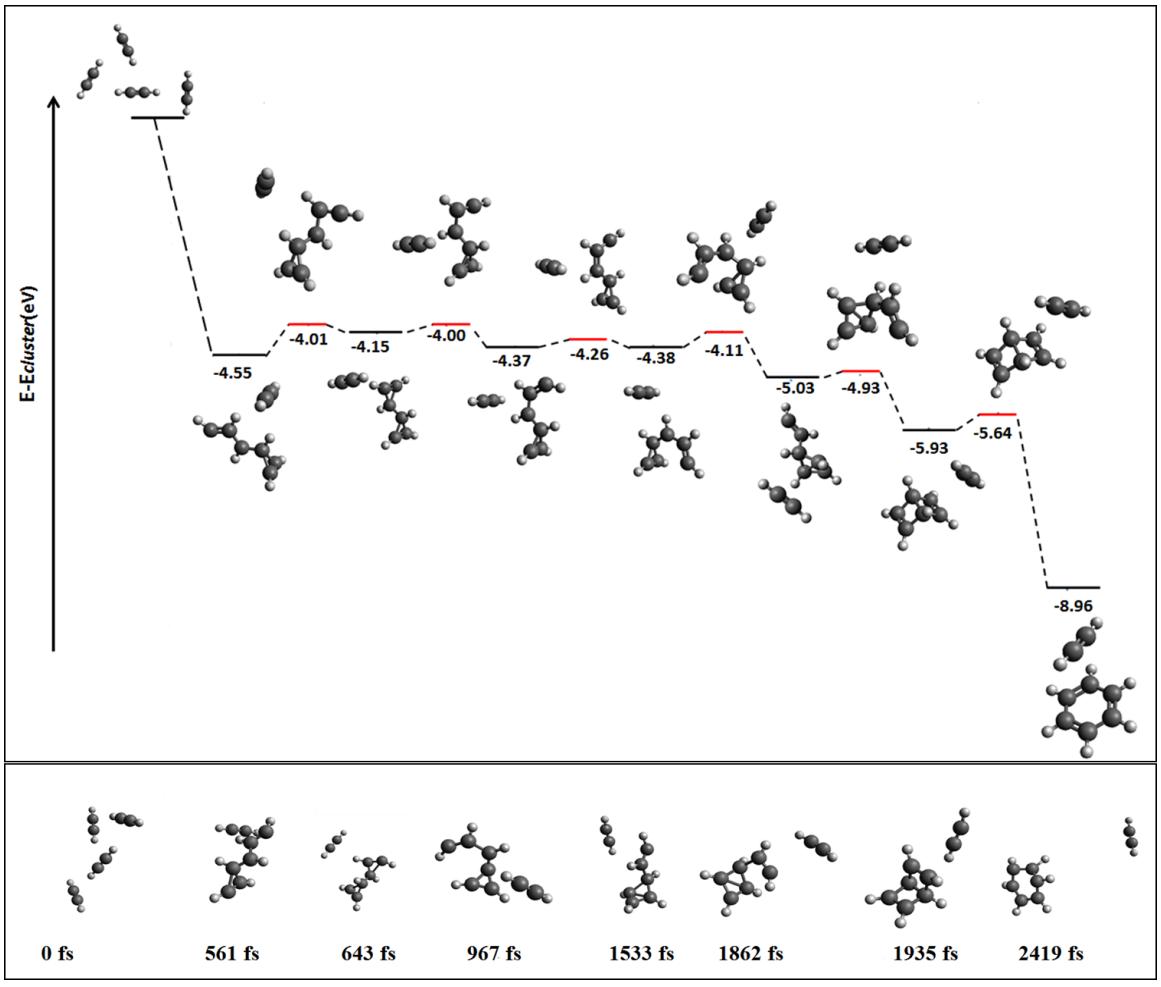

Figure 6: Top panel: Stationary points (saddle points in red) on a pathway leading to benzene cation from the ionized tetramer cluster. Relative energies (eV) of the different structures are with respect to the initial cluster geometry. Bottom panel: Snapshots from a trajectory leading to benzene cation formation from the tetramer cluster.

To further examine the catalytic role of the spectator acetylene molecules, we re-ran the trajectories that led to the formation of the benzene cation from the tetramer – however, this time starting only from the reactive 3 acetylene molecules (of the tetramer). This will enable us to assess the role played by the spectator acetylene molecule. We identified 5 different starting geometries of the reactive acetylene (that led to benzene in the tetramer) and as before ran 30 trajectories for each structure. The ratio between $C_6H_6^+$ and $C_4H_4^+$ products obtained is 0.13, which can be compared to the full tetramer trajectories in which the ratio is 0.27. The considerable difference in the product ratio indicates the non-trivial role of the free acetylene molecule in directly accessing $C_6H_6^+$ products.

For the pentamer clusters, a larger fraction (32%) of the trajectories (58 trajectories) ended up with a bonded $C_6H_6^+$ core. Figure 7 presents the ratio between $C_6H_6^+$ and $C_4H_4^+$ products as a function of the number of acetylene units in the cluster. For the pentamer and hexamer clusters, the ratio nearly doubles with respect to the trimer and tetramer clusters. This result can be partly attributed to the fact that there are additional acetylene molecules that are available for bonding. Moreover, the additional acetylene can further stabilize the forming structures. Among the 58 nascent $C_6H_6^+$ structures, 5 have the benzene cation structure. Snapshots from one of those trajectories, and corresponding stationary points are shown in Figure 8. The path in this example resembles the one for the trimer case. One can see that there is a reduction in the barriers due to the presence of the extra acetylene units, for example the barrier for the formation of benzene cation from benzvalene is 0.5 eV, where it was 0.6 in the trimer case. Both barriers are significantly less than the excess energy of the system (i.e. they are submerged).

There is an interesting reduction in the timescale necessary to access the benzene cation structure in the pentamer versus tetramer trajectories. In the tetramer case, all formation of benzene cation occurred after 1.2 ps, while for the pentamer, the benzene cation formation occurs roughly two to three times faster (we terminated these trajectories after 1.2 ps). This difference can be attributed to the additional stabilization and barrier lowering as a result of the presence of the extra acetylene. Moreover, we would expect additional benzene cation formation at later times (coming from other

gateway $C_6H_6^+$ structures). Indeed 33 of the $C_6H_6^+$ trajectories finished with core structures that can lead to benzene such as allyl-cyclopropenyl and vinyl-cyclobutadienyl cation structures. Similar considerations apply to the hexamer clusters: 32% of the trajectories led to $C_6H_6^+$ structures, of which 7 are the benzene cation, with another 21.5% (58 trajectories) that will probably lead to this species at later times. A fraction of these higher energy isomers could also be stabilized by rapid removal of sufficient internal energy prior to isomerization to benzene cation.

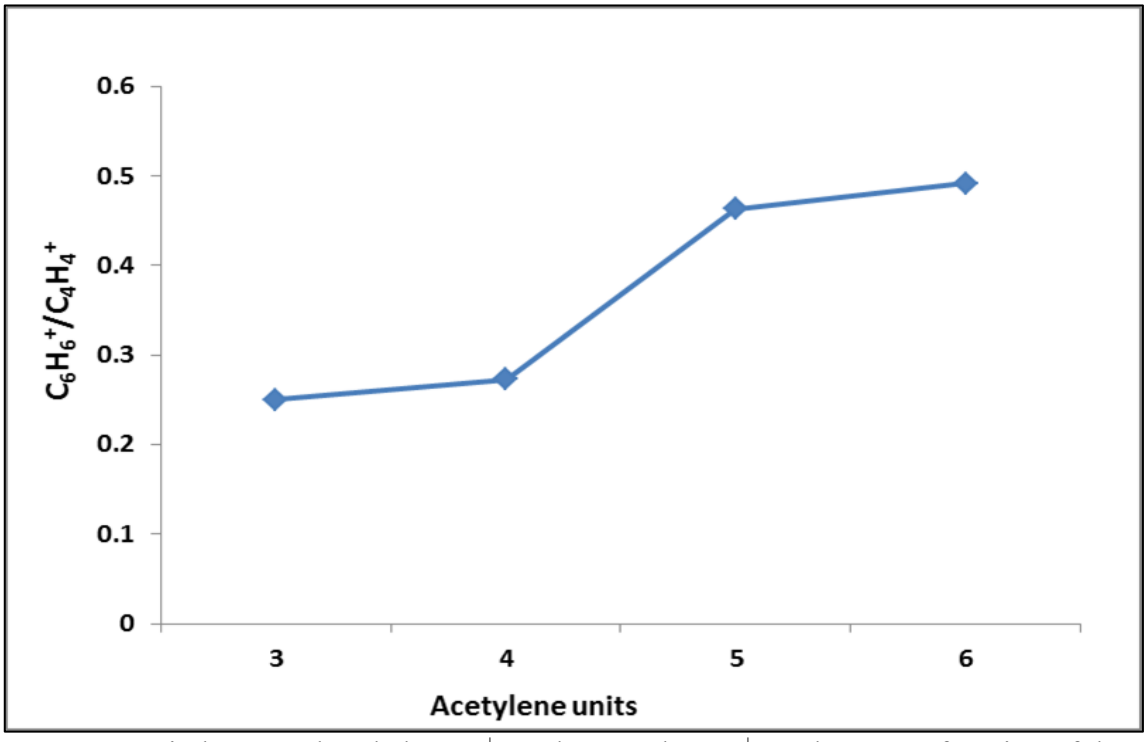

Figure 7: Ratio between bonded $C_6H_6^+$ products and $C_4H_4^+$ products as a function of the number of acetylene molecules in the cluster that is ionized. Note the substantial change in ratio as the cluster changes from trimer to tetramer, reflecting static and dynamical changes that are discussed in the text.

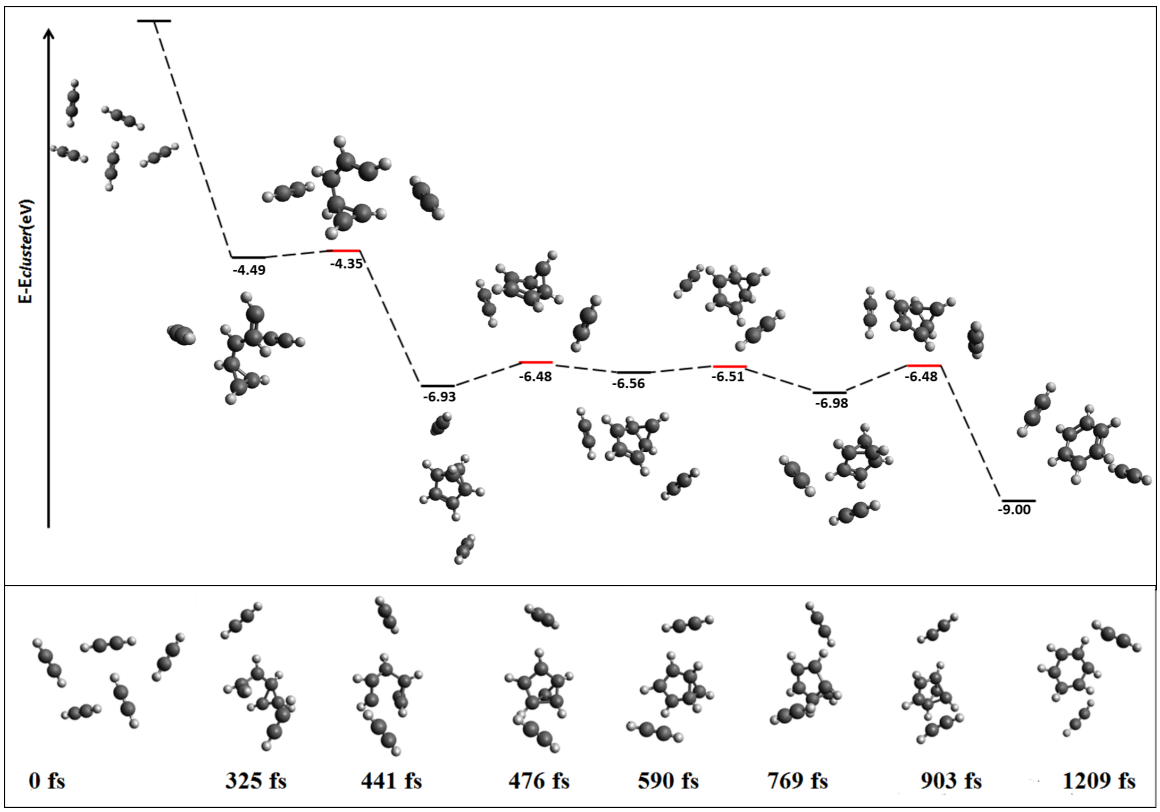

Figure 8: Top panel: Stationary points (saddle points in red) on a pathway leading to benzene cation from the ionized pentamer cluster. Relative energies (eV) of the different structures are with respect to the initial cluster geometry. Bottom panel: Snapshots from a trajectory leading to benzene cation formation from the ionized pentamer cluster.

Methods

Experimental

We used two experimental schemes – a) the ionization were carried out right after the nozzle exit at variable distances and then the beam was skimmed and sampled into the mass spectrometer ("in-source ionization"), and b) ionization where the beam is expanded, cooled, skimmed and ionized in the mass spectrometer chamber ("mass-spec ionization"). The schematics of these two experiments are shown in the insets of Figure 1. For both of these schemes, the experiments were carried out in a continuous supersonic expansion cluster machine coupled to a three meter VUV monochromator on the Chemical Dynamics Beamline (9.0.2), located at the Advanced Light Source, Berkeley, California. The experimental set up for both in-source and mass-spec ionization have been described separately in detail.(43, 49) For in-source ionization, 400 Torr of these

gas mixtures were expanded through a 100 μm nozzle to a differentially-pumped chamber kept at a pressure of 2×10^{-4} Torr. The beam was intersected with the VUV radiation at various axial distances from the nozzle (2-25 mm) and the resulting ions are sampled into a reflectron time-of-flight (ReTOF) mass spectrometer. The ionization distance was varied by changing the nozzle position with respect to the point of intersection of molecular and VUV beams. A set of four electrodes were used to guide the ions from the ionization region to the mass spectrometer through a skimmer. The lenses were kept at small potentials (+5, 0, -3, and 0 V, respectively) and the skimmer was grounded. The mass spectrometer was kept at 2×10^{-6} Torr in the second differentially-pumped chamber. A start pulse for the TOF was provided by pulsing both the repeller and accelerator plates because of the quasi-continuous (500 MHz) nature of the synchrotron light and investigation of the charged species. The ions were pulse-extracted by a fast switching of repeller and accelerator plates to 1100 and 1080V correspondingly.

For mass-spec ionization, 2000 Torr of 7% C_2H_2 in Ar was expanded and skimmed before ionization by tunable VUV at energies 11.0 – 15.0 eV. Varying percentages of acetylene were mixed with argon to compare the cluster distributions. Furthermore, various backing pressures (from 800 to 2500 Torr) were also used. The typical pressures of source and mass spectrometer chambers were 4.8×10^{-4} and 4.4×10^{-5} Torr.

The detection scheme for these two methods were the same. Ions were accelerated perpendicularly to their initial flight path through the field-free region and detected by a microchannel plate (MCP) detector installed at the end of the tube. The time dependent electrical signal from the detector was amplified by a fast preamplifier, collected by a multichannel scalar card, and then integrated with a computer. TOF spectra were measured at different positions in the photon energy range between 10 and 12 eV.

Theoretical

All calculation reported in this manuscript were carried out using Q-Chem 4.(50) Structures and relative energies were calculated using density functional theory (DFT). Geometry optimizations of the neutral and ionized cluster structures up to pentamers were carried out using the ωB97X-V functional(51), with the adequately large aug-cc-

pVTZ basis-set. Frequency calculations were performed to verify that the structures are fully relaxed. Geometry optimizations for the hexamer clusters were performed at the ωB97X-V/cc-pVDZ level. ωB97X-V is a range separated functional and as such reduces the self-interaction error(52, 53) and therefore is suitable for the description of the radical cation systems.(54) It also contains non-local correlation to accurately describe non-covalent interactions, and thus is also suitable for the treatment of the neutral acetylene clusters.

To gain more insight into the evolution of the ionized acetylene clusters, we also performed ab initio molecular dynamics (AIMD) simulations. The starting points of the calculations were the optimized neutral geometry on the cationic PES. For the AIMD calculation we used the ωB97 range-separated functional with the 6-31g* basis set for all clusters. The time step for the AIMD simulations was 1.21 fs (50 a.u) and the total simulation time was 1.2 ps (1000 time steps) unless stated otherwise. To account for different initial conditions of the clusters in the experiment, we ran 30 trajectories for each stable structure, starting from different low temperatures in the range of 30 to 80K.

Conclusions

In summary, we have computationally demonstrated that bonded $C_4H_4^+$ and $C_6H_6^+$ structures can form directly and barrierlessly after ionization of neutral acetylene clusters. Experimental results show that stable $C_4H_4^+$ and $C_6H_6^+$ structures can be formed from ionized clusters in a cold, collision-free regime. Ab initio molecular dynamics trajectories show $C_6H_6^+$ formation from clusters larger than the trimer due to the presence of additional acetylene molecules. The extra acetylene molecules stabilize the structures that form and lower the (submerged) barriers to their formation. Importantly, their evaporation allows for dissipation of the nascent hot $C_6H_6^+$ species. Our results correspond to a viable path for benzene cation formation in rich acetylene environments, which may be followed by scavenging free electrons to yield benzene, and subsequently, PAHs. This is relevant for the formation of benzene in the ISM, where acetylene is abundant, and can also play a role in acetylene rich flames, where the cation can also be found. Future work will seek to generate larger PAH species by performing experiments

and theoretical calculations on benzene/toluene clusters and probing them with VUV photoionization mass spectrometry coupled to ab-initio calculations.

Acknowledgements: TS, MA, BB, OK, YF, TPT, MHG and the Advanced Light Source are supported by the Director, Office of Science, Office of Basic Energy Sciences, of the U.S. Department of Energy under Contract No. DE-AC02-05CH11231. TS and MHG acknowledge additional support from the National Aeronautics and Space Administration through the NASA Astrobiology Institute under Cooperative Agreement Notice NNH13ZDA017C issued through the Science Mission Directorate.

References

1. Ehrenfreund P & Sephton MA (2006) Carbon molecules in space: from astrochemistry to astrobiology. *Farad. Discuss.* 133(0):277-288.
2. Rhee YM, Lee TJ, Gudipati MS, Allamandola LJ, & Head-Gordon M (2007) Charged polycyclic aromatic hydrocarbon clusters and the galactic extended red emission. *Proc. Natl. Acad. Sci. U.S.A.* 104(13):5274-5278.
3. Joblin C & Mulas G (2009) Interstellar polycylic aromatic hydrocarbons: from space to the laboratory. *Eas Publications* 35:133-152.
4. Larsen JC & Larsen PB (1998) Chemical Carcinogens. *Air Pollution and Health*, eds Hester RE & Harrison RM (The Royal Society of Chemistry), Vol 10, pp 33-56.
5. Baek SO*, et al.* (1991) A review of atmospheric polycyclic aromatic hydrocarbons: sources, fate and behavior. *Water Air Soil Pollut.* 60(3):279-300.
6. Puget JL & Léger A (1989) A new component of the interstellar matter: small grains and large aromatic molecules. *Annu. Rev. Astron. Astrophys.* 27(1):161-198.
7. Richter H & Howard JB (2000) Formation of polycyclic aromatic hydrocarbons and their growth to soot—a review of chemical reaction pathways. *Prog. Energy Combust. Sci.* 26(4–6):565-608.
8. Frenklach M & Wang H (1991) Twenty-Third Symposium (International) on CombustionDetailed modeling of soot particle nucleation and growth. *Symp. Int. Combust.* 23(1):1559-1566.
9. Bittner JD & Howard JB (1981) Eighteenth Symposium (International) on Combustion Composition profiles and reaction mechanisms in a near-sooting premixed benzene/oxygen/argon flame. *Symp. Int. Combust.* 18(1):1105-1116.
10. Wang H & Frenklach M (1994) Calculations of rate coefficients for the chemically activated reactions of acetylene with vinylic and aromatic radicals. *J. Phys. Chem.* 98(44):11465-11489.
11. Marinov NM*, et al.* (1998) Aromatic and polycyclic aromatic hydrocarbon formation in a laminar premixed n-butane flame. *Combust. Flame* 114(1–2):192-213.
12. Parker DSN, Kaiser RI, Troy TP, & Ahmed M (2014) Hydrogen abstraction/acetylene addition revealed. *Angew. Chem. Int. Ed.* 53(30):7740-7744.
13. Hopf H (2004) From acetylenes to aromatics: novel routes – novel products. *Modern Arene Chemistry*, (Wiley-VCH Verlag GmbH & Co. KGaA), pp 169-195.

14. El-Shall MS (2008) Polymerization in the gas phase, in clusters, and on nanoparticle surfaces. *Acc. Chem. Res.* 41(7):783-792.
15. Momoh PO*, et al.* (2014) Formation of covalently bonded polycyclic hydrocarbon ions by Intracluster polymerization of ionized ethynylbenzene clusters. *J. Phys. Chem. A* 118(37):8251-8263.
16. Parker DSN*, et al.* (2012) Low temperature formation of naphthalene and its role in the synthesis of PAHs (Polycyclic Aromatic Hydrocarbons) in the interstellar medium. *Proc. Natl. Acad. Sci.* 109(1):53-58.
17. Ghesquière P & Talbi D (2013) On the formation of naphthalene cation in space from small hydrocarbon molecules: A theoretical study. *Chem. Phys. Lett.* 564:11-15.
18. Paul MW & Karen W (2007) Benzene formation in the inner regions of protostellar disks. *Astrophys. J. Lett.* 655(1):L49.
19. Woods PM (2011) The formation of benzene in dense environments. *EAS Publications Series* 46:235-240.
20. C. Brown RF (1999) Some developments in the high temperature gas phase chemistry of alkynes, arynes and aryl radicals. *European Journal of Organic Chemistry* 1999(12):3211-3222.
21. Hopf H*, et al.* (1997) Formation of isobenzenes by thermal isomerization of 1,3-hexadiene-5-yne derivatives. *Angewandte Chemie International Edition in English* 36(11):1187-1190.
22. Cuylle SH, Zhao D, Strazzulla G, & Linnartz H (2014) Vacuum ultraviolet photochemistry of solid acetylene: a multispectral approach. *A&A* 570:A83.
23. Miller JA & Klippenstein SJ (2003) The recombination of propargyl radicals and other reactions on a C6H6 potential. *J. Phys. Chem. A* 107(39):7783-7799.
24. Miller JA & Melius CF (1992) Kinetic and thermodynamic issues in the formation of aromatic compounds in flames of aliphatic fuels. *Combust. Flame* 91(1):21-39.
25. Cole JA, Bittner JD, Longwell JP, & Howard JB (1984) Formation mechanisms of aromatic compounds in aliphatic flames. *Combust. Flame* 56(1):51-70.
26. Frenklach M & Warnatz J (1987) Detailed modeling of PAH profiles in a sooting low-pressure acetylene flame. *Combust. Sci. Technol.* 51(4-6):265-283.
27. Harris SJ, Weiner AM, & Blint RJ (1988) Formation of small aromatic molecules in a sooting ethylene flame. *Combust. Flame* 72(1):91-109.
28. Murray JM*, et al.* (1999) New H and H2 reactions with small hydrocarbon ions and their roles in benzene synthesis in dense interstellar clouds. *Astrophys. J.* 513(1):287.
29. Paul MW, Millar TJ, Zijlstra AA, & Eric H (2002) The synthesis of benzene in the proto-planetary nebula CRL 618. *Astrophys. J. Lett.* 574(2):L167.
30. Kaiser RI, Parker DSN, & Mebel AM (2015) Reaction dynamics in astrochemistry: low-temperature pathways to polycyclic aromatic hydrocarbons in the interstellar medium. *Annu. Rev. Phys. Chem.* 66(1):43-67.
31. Yang Y*, et al.* (2012) Mechanism for the formation of benzene in the Titan's atmosphere: A theoretical study on the mechanism of reaction. *Comp. Theor. Chem.* 991:66-73.
32. Jones BM*, et al.* (2011) Formation of benzene in the interstellar medium. *Proc. Natl. Acad. Sci.* 108(2):452-457.
33. Li Z*, et al.* (2010) Cosmic-ray mediated formation of benzene on the surface of saturn's moon titan. *Astrophys. J.* 718(2):1243.
34. Shinohara H, Sato H, & Washida N (1990) Photoionization mass spectroscopic studies of ethylene and acetylene clusters: intracluster excess energy dissipation. *J. Phys. Chem.* 94(17):6718-6723.

35. Tzeng WB, Ono Y, Linn SH, & Ng CY (1985) A study of the unimolecular decomposition of the (C2H4)+3 complex. *J. Chem. Phys.* 83(6):2813-2817.
36. Booze JA & Baer T (1993) The photoionization and dissociation dynamics of energy-selected acetylene dimers, trimers, and tetramers. *J. Chem. Phys.* 98(1):186-200.
37. Kočišek J, Lengyel J, & Fárník M (2013) Ionization of large homogeneous and heterogeneous clusters generated in acetylene–Ar expansions: cluster ion polymerization. *J. Chem. Phys.* 138(12):124306.
38. Coolbaugh MT, Whitney SG, Vaidyanathan G, & Garvey JF (1992) Intracluster polymerization reactions within acetylene and methylacetylene clusters ions. *J. Phys. Chem.* 96(23):9139-9144.
39. Ono Y & Ng CY (1982) A study of the unimolecular decomposition of the (C2H2)3+ complex. *J. Am. Chem. Soc.* 104(18):4752-4758.
40. Momoh PO, Abrash SA, Mabrouki R, & El-Shall MS (2006) Polymerization of ionized acetylene clusters into covalent bonded ions: evidence for the formation of benzene radical cation. *J. Am. Chem. Soc.* 128(38):12408-12409.
41. Momoh PO & El-Shall MS (2007) Stepwise hydration of ionized acetylene trimer. Further evidence for the formation of benzene radical cation. *Chem. Phys. Lett.* 436(1–3):25-29.
42. Relph RA, Bopp JC, Roscioli JR, & Johnson MA (2009) Structural characterization of (C2H2)1–6+ cluster ions by vibrational predissociation spectroscopy. *J. Chem. Phys.* 131(11):114305.
43. Bandyopadhyay B, Kostko O, Fang Y, & Ahmed M (2015) Probing methanol cluster growth by vacuum ultraviolet ionization. *J. Phys. Chem. A* 119(18):4083-4092.
44. Bandyopadhyay B*, et al.* (2016) Probing ionic complexes of ethylene and acetylene with vacuum-ultraviolet radiation. *J. Phys. Chem. A* 120(27):5053-5064.
45. Pauly H (2000) *Molecule and Cluster Beams I* (Springer-Verlag, Berlin, Germany).
46. Momoh PO, Hamid AM, Abrash SA, & Samy El-Shall M (2011) Structure and hydration of the C4H4•+ ion formed by electron impact ionization of acetylene clusters. *J. Chem. Phys.* 134(20):204315.
47. Momoh PO, Hamid AM, Soliman A-R, Abrash SA, & El-Shall MS (2011) Structure of the C8H8•+ radical cation formed by electron impact ionization of acetylene clusters. Evidence for a (Benzene•+·Acetylene) complex. *J. Phys. Chem. Lett.* 2(19):2412-2419.
48. Bera PP, Head-Gordon M, & Lee TJ (2013) Association mechanisms of unsaturated C2 hydrocarbons with their cations: acetylene and ethylene. *Phys. Chem. Chem. Phys.* 15(6):2012-2023.
49. Kostko O, Belau L, Wilson KR, & Ahmed M (2008) Vacuum-ultraviolet (VUV) photoionization of small methanol and methanol−water clusters. *J. Phys. Chem. A* 112(39):9555-9562.
50. Shao Y*, et al.* (2015) Advances in molecular quantum chemistry contained in the Q-Chem 4 program package. *Mol. Phys.* 113(2):184-215.
51. Mardirossian N & Head-Gordon M (2014) [small omega]B97X-V: A 10-parameter, range-separated hybrid, generalized gradient approximation density functional with nonlocal correlation, designed by a survival-of-the-fittest strategy. *Phys. Chem. Chem. Phys.* 16(21):9904-9924.
52. Chai J-D & Head-Gordon M (2009) Long-range corrected double-hybrid density functionals. *J. Chem. Phys.* 131(17):174105.
53. Kronik L, Stein T, Refaely-Abramson S, & Baer R (2012) Excitation gaps of finite-sized systems from optimally tuned range-separated hybrid functionals. *J. Chem. Theory Comput.* 8(5):1515-1531.

54. Livshits E, Granot RS, & Baer R (2011) A density functional theory for studying ionization processes in water clusters. *J. Phys. Chem. A* 115(23):5735-5744.

Figure Legends

Figure 1: Mass spectra of acetylene clusters obtained from in-source (a) and mass-spec ionization (b) at 11.5 eV. The experimental schemes are graphically shown in the insets. While in-source ionization shows fragmented acetylene clusters (e.g. $C_4H_3^+$, $C_6H_5^+$), mass-spec ionization shows intact clusters in the form of $(C_2H_2)_n^+$.

Figure 2: Optimized low-energy structures of neutral acetylene clusters. Tr: trimer structures, T: tetramer structures, P: pentamer structures. Binding energies (kJ/mol) are shown for each relaxed structure.

Figure 3: Structures of the ionized clusters upon relaxation starting from each optimized neutral structure shown in Figure 2. The isomer labels correspond to those shown in Figure 2. Tr: resulting trimer structures, T: resulting tetramer structures, P: resulting pentamer clusters.

Figure 4: Top panel: Stationary points (saddle points in red) on a pathway leading to benzene cation from the ionized trimer cluster. Relative energies (eV) of the different structures are with respect to the initial cluster geometry. Bottom panel: Snapshots from a trajectory leading to benzene cation formation from the trimer cluster.

Figure 5: Time-dependence of the shortest CC distance between the nascent $C_4H_4^+$ or $C_6H_6^+$ structure and the most remote remaining acetylene molecule (which is defined at the end of the trajectory). An example of the CC distance is shown at the top left.

Figure 6: Top panel: Stationary points (saddle points in red) on a pathway leading to benzene cation from the ionized tetramer cluster. Relative energies (eV) of the different structures are with respect to the initial cluster geometry. Bottom panel: Snapshots from a trajectory leading to benzene cation formation from the tetramer cluster.

Figure 7: Ratio between $C_6H_6^+$ products and $C_4H_4^+$ products as a function of the number of acetylene molecules in the cluster that is ionized. Note the substantial change in ratio as the cluster changes from trimer to tetramer, reflecting static and dynamical changes that are discussed in the text.

Figure 8: Top panel: Stationary points (saddle points in red) on a pathway leading to benzene cation from the ionized pentamer cluster. Relative energies (eV) of the different structures are with respect to the initial cluster geometry. Bottom panel: Snapshots from a trajectory leading to benzene cation formation from the ionized pentamer cluster.

Supporting Information

Table S1: Calculated Vertical and Adiabatic Ionization Energies of the different clusters presented in the manuscript.

Structure (isomer)	Vertical IE (eV)	Adiabatic IE (eV)
$(C_2H_2)_3$	11.03	9.33
$(C_2H_2)_4$ (b)	10.92	6.91
$(C_2H_2)_4$ (c)	10.61	6.44
$(C_2H_2)_4$ (d)	10.98	6.39
$(C_2H_2)_4$ (e)	11.07	6.66
$(C_2H_2)_5$ (a)	10.90	6.24
$(C_2H_2)_5$ (c)	10.87	6.65
$(C_2H_2)_5$ (d)	10.92	6.58
$(C_2H_2)_5$ (e)	10.93	6.39
$(C_2H_2)_5$ (f)	10.79	6.76

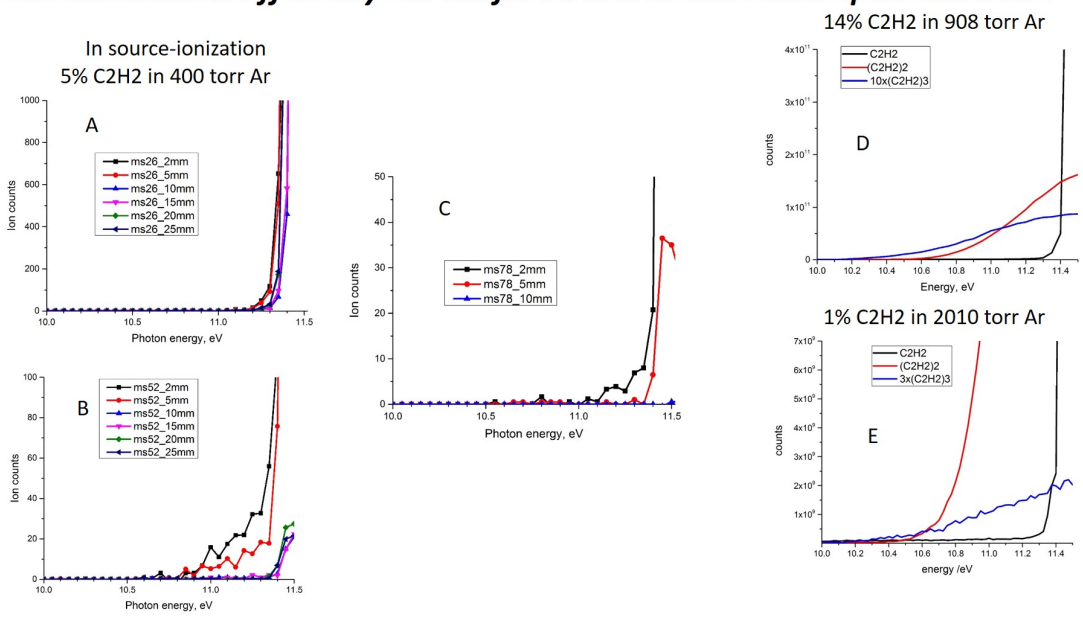

Figure S1. Photoionization efficiency curves for in-source and mass-spec ionization. In-source ionization is shown at various nozzle-ionization distances for 5% C_2H_2 in 400 Torr Ar (A) m/z 26 (C_2H_2), (B) m/z 52 (C_4H_4), (C) m/z 78 (C_6H_6), (D) mass spec ionization of 14% C_2H_2 in 908 Torr Ar showing m/z 26, 52, and 78; (E) mass spec ionization of 1% C_2H_2 in 2010 Torr Ar showing m/z 26, 52, and 78.

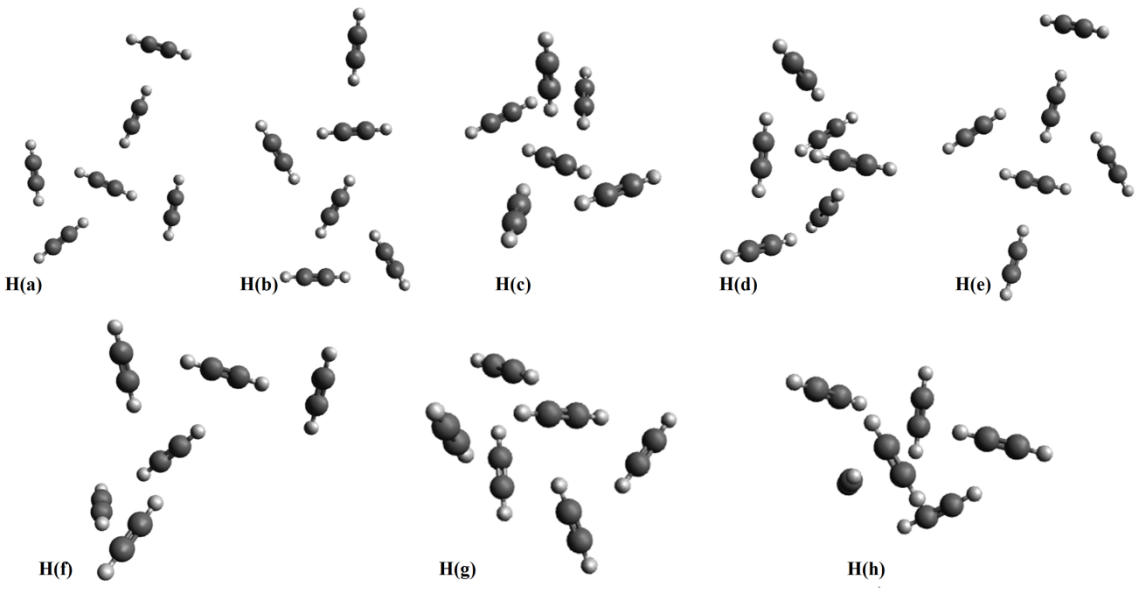

Figure S2: Structure of neutral hexamer clusters.

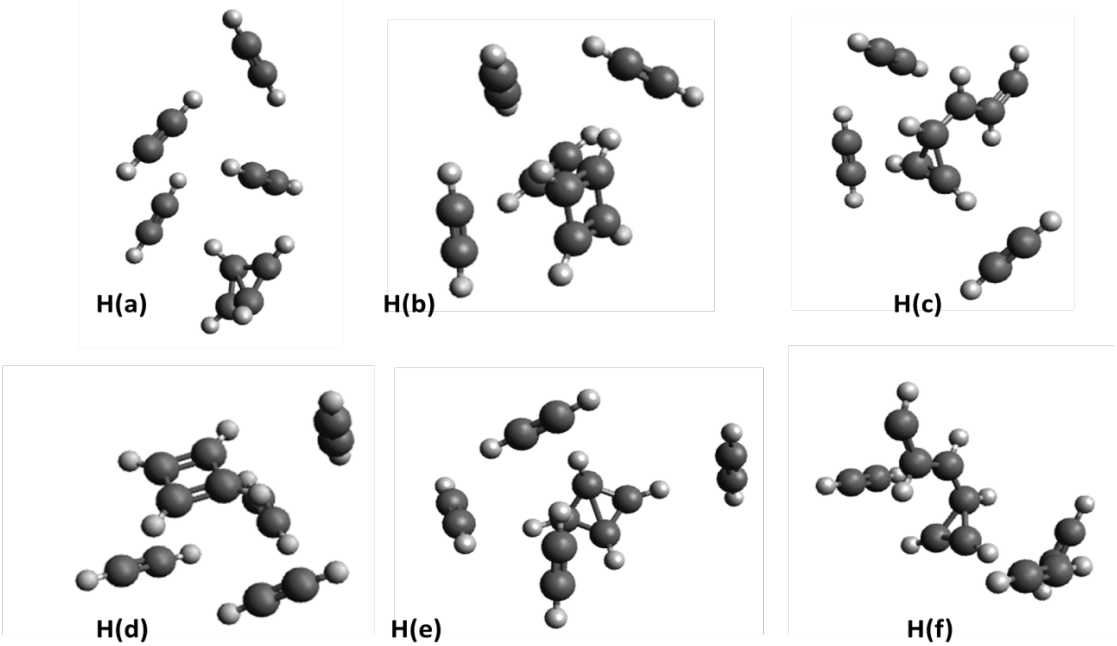

Figure S3: Structures of the hexamers upon relaxation on the cation surface.

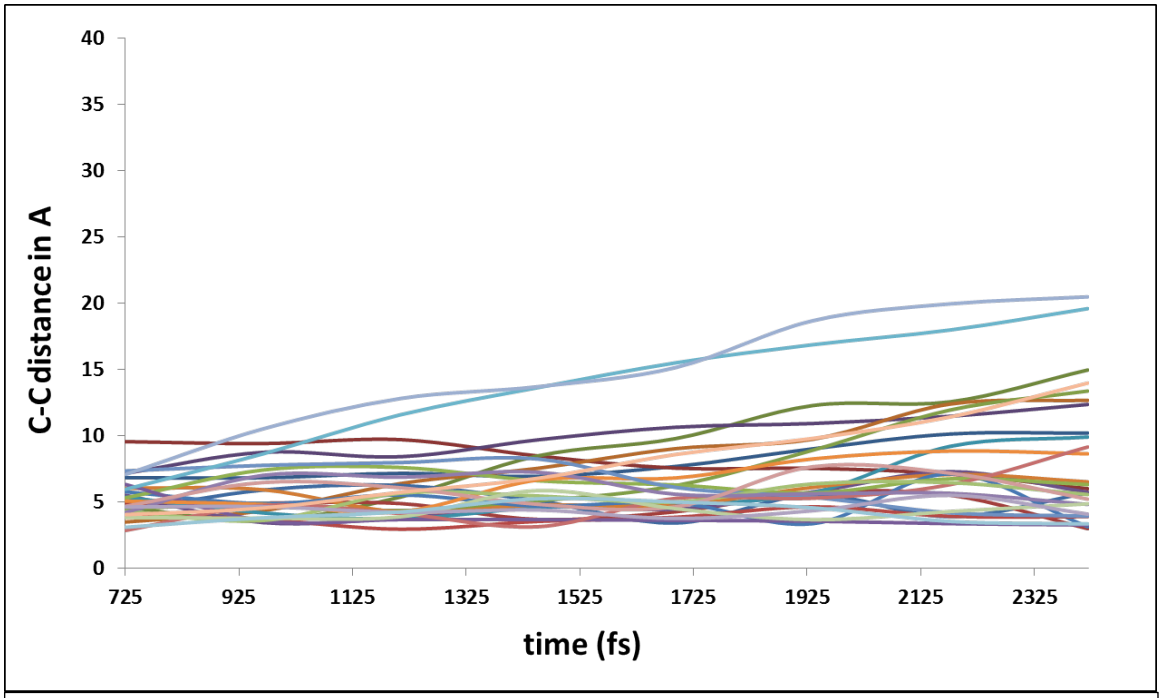

Figure S4: Time-dependence of the shortest CC distance between the nascent $C_4H_4^+$ or and the second-most remote actetylene molecule (which is identified at the end of the trajectory). This information supplements Figure 5 in the main text, which shows the shortest distance to the most remote acetylene. Dissociation of these solvating acetylene molecules is a mechanism for carrying away some of the internal energy of the bonded complexes.